

The Impact of Coastal Boundaries and Small Hills on the Precipitation Distribution across Southern Connecticut and Long Island, New York

BRIAN A. COLLE

Institute for Terrestrial and Planetary Atmospheres, Stony Brook University, Stony Brook, New York

SANDRA E. YUTER

Department of Marine, Earth, and Atmospheric Sciences, North Carolina State University, Raleigh, North Carolina

(Manuscript received 1 March 2006, in final form 12 June 2006)

ABSTRACT

The modification of precipitation by the coastal land areas of Long Island (LI), New York, and southern Connecticut (CT) is examined for an extratropical cyclone over the northeast United States on 1 December 2004, which produced strong southerly flow ($15\text{--}30\text{ m s}^{-1}$) below 900 mb and heavy precipitation over LI. The differential surface roughness at the coast and the hills of LI (30–80 m) and southern CT (100–250 m) enhanced the surface precipitation by 30%–50% over these regions compared with the nearby water region of LI Sound. The three-dimensional precipitation structures are shown using composite Weather Surveillance Radar-1988 Doppler radar data interpolated to a Cartesian grid, which is compared with a 4-km simulation using the fifth-generation Pennsylvania State University–National Center for Atmospheric Research Mesoscale Model (MM5). As the low-level stratification and flow increased at low levels, the MM5 produced a terrain-forced gravity wave over LI and CT upward through 6 km MSL. Precipitation enhancement (2–3 dBZ) occurred from the surface upward to around the freezing level (3 km MSL) across central LI and southern CT, while there was a localized precipitation minimum over LI Sound. A factor separation on a few sensitivity MM5 runs was performed to isolate the impact of small hills and differential friction across the LI coastline. Both the hills and frictional effects have similar contributions to the total precipitation enhancement and the vertical circulations below 3 km. The hills of LI enhanced the gravity wave circulations slightly more than the differential friction above 3 km, while there was little flow and precipitation interaction between the hills and differential friction. A sensitivity simulation without an ice/snow cloud above 3 km MSL revealed that the seeder-feeder process enhanced surface precipitation by about a factor of 4.

1. Introduction

a. Background

The impact of topography on the spatial distribution of precipitation has been the focus of numerous research studies over several decades. As reviewed by Smith (1979) and Houze (1993), precipitation can be enhanced near orography via forced lifting, upstream flow blocking, mountain gravity waves aloft, convective circulations induced by mountain–valley thermal gradients, and leeside convergence. Most previous studies

have investigated relatively steep and high barriers (e.g., the Rocky Mountains, the Cascade Mountains, the Alps, and the Appalachian Mountains), which produce significant low-level flow perturbations.

It is also well known that precipitation can become enhanced via a “seeder-feeder” mechanism over relatively small (50–200 m) hills (Bergeron 1949, 1960; Storebo 1976). During this process, precipitation particles falling from aloft (seeder clouds) grow as they collect small cloud droplets within the low-level (feeder) cap cloud over a hill. This seeder-feeder process has been duplicated using model simulations of moist airflow over 400-m hills (Bader and Roach 1977).

Precipitation enhancement over relatively small hills has been observed over south Wales (Browning 1980; Hill et al. 1981), central Pennsylvania (Barros and Ku-

Corresponding author address: Dr. Brian A. Colle, Marine Sciences Research Center, Stony Brook University, Stony Brook, NY 11794-5000.

E-mail: brian.colle@stonybrook.edu

ligowski 1998), and southern New England (Passarelli and Boehme 1983). During these events there is typically strong and moist cross-barrier flow, which creates a liquid or cloud ice layer just over the hill, while an approaching frontal system generates the snow aloft. Passarelli and Boehme (1983) showed that the precipitation over the 100–400-m hills of southern New England is often enhanced by 20%–60% when low-level easterly flow impinges toward the north–south-orientated terrain ahead of an approaching warm frontal system.

Passarelli and Boehme (1983) also noted that there was a 10%–20% enhancement of precipitation over the coastal plain of southern New England, which is a region with <100-m hills. They hypothesized that the coastal enhancement may result from frictional convergence associated with stronger winds rapidly decelerating at the coast (e.g., Bergeron 1949) as well as the gentle upward slope of the coastal plain. They noted that the average slope is $\sim 0.2\%$, which can result in an upslope vertical velocity of 2 cm s^{-1} for an ambient flow of 10 m s^{-1} , while the vertical motion from frictional convergence was estimated to be $\sim 10 \text{ cm s}^{-1}$ at the coast.

Braun et al. (1999) conducted two-dimensional idealized simulations to illustrate the vertical motions produced by differential friction at the coast. They showed that a rapid deceleration of the onshore flow at the coast leads to an increase in boundary layer depth and a narrow zone of upward motion, which in turn forces a vertically propagating gravity wave above the coast. However, they did not investigate the impact this gravity wave may have on the precipitation.

b. Motivation

Although the Passarelli and Boehme (1983) observational analysis did not include Long Island (LI), the primary region of interest for this paper, the same small hill and frictional convergence hypotheses may operate. Long Island has 50–80-m hills across the central parts of the island (Fig. 1) that are associated with a glacial terminal moraine. The impact of the LI hills on precipitation has not been previously addressed. Furthermore, under southerly low-level flow, the west–east geometry of LI may also create frictional convergence and divergence along the south and north shores, respectively, which can further modify the precipitation. Meanwhile, the opposite convergence and divergence pattern occurs for northerly flow.

There have been few precipitation climatologies across LI on a small-scale, since high-density surface observations in this area have only recently been synthesized (Novak and Colle 2006). Miller and Frederick

(1969) used 20–30 cooperative observer stations over a 15-yr period (1951–65) to show that the precipitation was 10%–20% greater across central portions of LI than the adjacent north and south shores during the cool season. This is consistent with Colle et al. (2003), who showed by using the fifth-generation Pennsylvania State University–National Center for Atmospheric Research (PSU–NCAR) Mesoscale Model (MM5) at 4-km grid spacing that the precipitation over central LI during the 1999–2001 cool seasons was enhanced by about 10%–15% as compared to the adjacent Atlantic Ocean waters to the south (see their Fig. 2c).

The simulated precipitation enhancement over LI is smaller than the 20%–60% documented for southern New England for the cool season, but an important question is under what conditions the LI precipitation enhancement is much greater than the climatological average value of 10%–20%. Long Island is unique geographically, since it has both small hills and is surrounded by water except on its western end. Additional motivation to investigate precipitation over relatively low hills originates from recent radar observations and modeling results by Garvert et al. (2005, 2006, manuscript submitted to *Mon. Wea. Rev.*), which showed that narrow and relatively small (300–500 m) terrain peaks of the central Oregon Cascades can produce vertically propagating gravity waves during strong ($>20 \text{ m s}^{-1}$) cross-barrier flow. These gravity waves created plumes of high liquid water content and snow production upward to 600 mb. The LI terrain is much lower than 300–500 m, but can the hills of LI also produce large enough gravity waves to impact the microphysical processes aloft? The results of Braun et al. (1999) suggest that differential friction at the coast may be enough to generate a vertically propagating gravity wave, so this response also needs to be investigated.

This study examines a heavy precipitation event over LI on 1 December 2004, during which record daily rainfall totals were set at LaGuardia Airport (2.64 cm), JFK Airport (1.60 cm), and Islip, LI (2.11 cm). Figure 2a shows the Weather Surveillance Radar-1988 Doppler (WSR-88D) radar storm total estimate between 0600 UTC 1 December and 1500 UTC 1 December 2004, while Fig. 2b shows a contoured analysis of the available precipitation gauge reports. For this event a band of enhanced precipitation amounts extended west–east across central LI, with around 25 mm across north-central portions of the island. In contrast, radar estimates suggest that only around 10–12 mm fell over the adjacent waters of the Atlantic and Long Island Sound (LIS). Another area of precipitation enhancement (to 25–30 mm) was over coastal Connecticut (CT). This 30%–50% precipitation enhancement across LI and

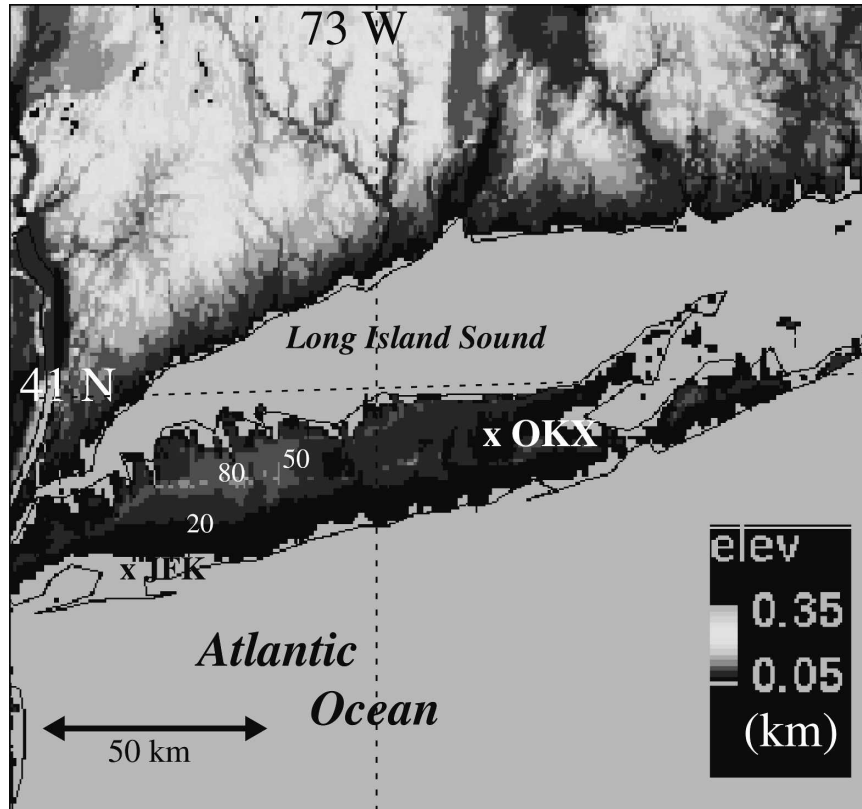


FIG. 1. Topographic map (shaded in km) of the region. The Upton, NY, radar used in this study is shown at OKX. Other geographic points are also labeled as well as some critical elevations (m) over LI.

coastal CT nearly follows the coastal geometry, suggesting some potentially important dynamical impacts from the land–water differential friction. To investigate this event, section 2 describes the observational datasets and simulation methods used to analyze the precipitation evolution. The large-scale and mesoscale analysis will be presented in section 3. Additional discussion and sensitivity runs were completed to separate the differential friction and terrain effects in section 4. Section 5 gives the conclusions.

2. Data and methods

a. Observational datasets

This study utilized conventional surface and rawinsonde observations, Aircraft Communications Addressing and Reporting System (ACARS) data, as well as the level-II reflectivity and radial velocity data¹ from the WSR-88D radar at Upton, New York (NY) (OKX

in Fig. 1). This coastal radar allows for the unique vertical sampling of precipitation systems as they cross LI and southern New England.

The WSR-88D polar coordinate radar data were converted from level-II format to Universal Format (UF) format (Barnes 1980). The UF format data were processed to dealias radial velocities (James et al. 2000) and then interpolated to three-dimensional Cartesian grids utilizing NCAR Earth Observing Laboratory's REORDER software with Cressman weighting. Two radar data grids were used for this study: a grid with 2-km horizontal and 0.5-km vertical spacing to a 75-km range for use in detailed three-dimensional comparisons with model output, and a coarser grid with 4-km horizontal and 1-km vertical spacing out to 230-km range used to show regional patterns of low-level reflectivity. The interpolated Cartesian data were converted to Unidata's Network Common Data Format (netcdf) for display using *Mountain Zebra* (James et al. 2000), which is a version of NCAR's *Zebra* software (Corbet et al. 1994), and for further processing. Mean reflectivities were computed for three 2-h periods using the interpolated radar volumes between 0900 and 1500

¹ Radar data were obtained from the National Climatic Data Center.

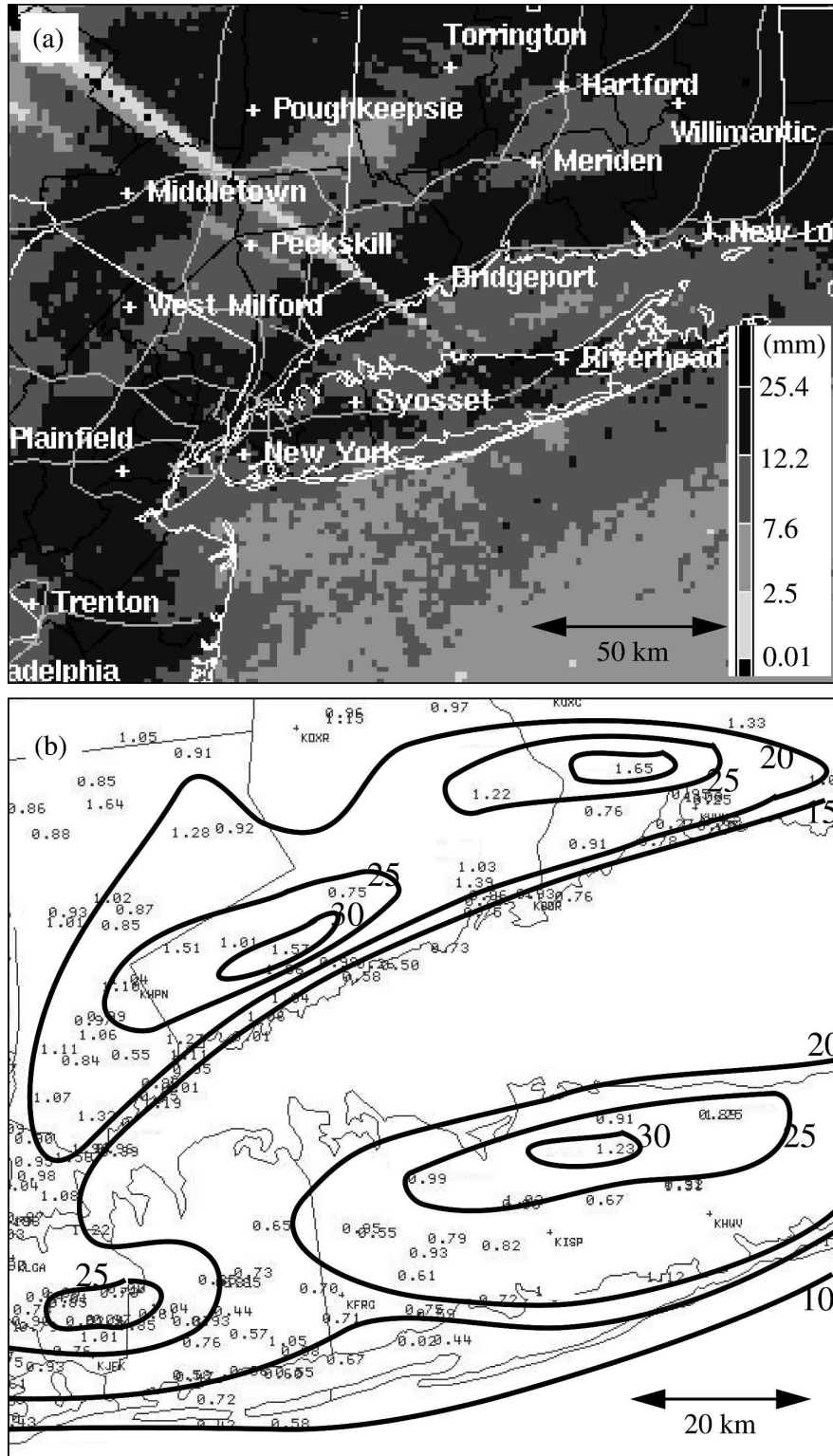


FIG. 2. (a) Radar (KOKX) estimated precipitation (shaded, mm) between 0600 and 1800 UTC 1 Dec 2004. (b) Rain gauge precipitation (solid every 5 mm) between 0600 and 1800 UTC 1 Dec 2004. The rain gauge reports are plotted individually (in.) for reference.

UTC, which is the period of heaviest rainfall across LI. The radial velocities were not utilized across western LI, since the low-level (southerly) flow across the island was nearly normal to the radar beam; however, the velocities were useful to diagnose flow perturbations to the north of OKX across LIS and southern coastal CT.

b. Model setup

The MM5 (version v3.6) was used in nonhydrostatic mode in order to provide additional data for diagnosing the structural evolution and associated precipitation structures around LI. For this simulation, stationary 1.33-, 4-, and 12-km domains were nested within a 36-km domain using a one-way nested interface (Fig. 3a). This study will focus primarily on the 4-km results, since it will be shown below that the 4- and 1.33-km grids produce similar precipitation structures across LI. Therefore, to limit the computational requirements for the several sensitivity simulations discussed in section 4, only the 4-km nest was used. The model top was set at 100 mb. Thirty-three unevenly spaced full-sigma levels were used in the vertical, with the maximum resolution in the boundary layer. Five-minute-averaged terrain data were analyzed to the 36- and 12-km model grids using a Cressman analysis scheme and filtered by a two-pass smoother/desmoother. For the 4-km domain (Fig. 3b), a 30-s topography dataset was interpolated to the grid in order to better resolve the inland hills and valleys. A 30-s land-use dataset from NCAR was used to initialize 25 surface categories for all domains. Initial atmospheric conditions at 0000 UTC 1 December 2004 were generated by interpolating the National Centers for Environmental Prediction (NCEP) Eta Model 221 grids (32-km grid spacing) to the MM5 grid. Additional analyses generated in the same manner using the 3-hourly Eta forecasts were linearly interpolated in time in order to provide the evolving lateral boundary conditions for the 36-km domain.

The U.S. Navy Optimum Thermal Interpolation System (OTIS) sea surface temperature analyses (~30-km grid spacing) were used to initialize the MM5 surface temperatures over water. The control (CTL) simulation used the Thompson microphysical scheme (Thompson et al. 2004), which includes prognostic equations for cloud ice and water, snow, graupel, and rain. The Grell convective parameterization (Grell et al. 1994) was applied, except for the 4- and 1.33-km domains, where convective processes could be resolved explicitly. Other parameterizations included NCEP's medium-range forecast (MRF) boundary layer scheme (Hong and Pan 1996), a long- and shortwave atmospheric radiation scheme (Dudhia 1989), and a radiative upper boundary condition (Klemp and Durran 1983).

3. Synoptic and mesoscale analysis

a. Synoptic overview

As the heavy precipitation developed around LI at 1200 UTC 1 December 2004, there was a well-defined shortwave trough at 500 mb approaching the northeast United States (Fig. 4a). The 500-mb winds exceeded 50 m s^{-1} around West Virginia, with well-defined diffluent flow to the east of the trough over Pennsylvania. The associated surface cyclone (992 mb) was near western NY (Fig. 4b), with an occluded front extending southward across western Pennsylvania and a cold front extending farther southward toward the Carolinas. The southerly flow along the East Coast advected relatively warm air northward across New England and was associated with a broad area of light-to-moderate precipitation reports across the northeast United States at this time (Fig. 4b). The strength of the surface cyclone in the MM5 at the same time in the simulation (hour 12) was within 2 mb and the position of the surface fronts was well simulated (Fig. 3a).

During the next 3–4 h the surface low moved northeastward to northern NY (not shown). Meanwhile, the occluded front approached and moved across LI, thus ending the heavy precipitation across LI by 1600 UTC 1 December and veering the surface winds to more westerly.

b. Mesoscale analysis

At the time of heaviest precipitation (1400 UTC 1 December), there was strong southerly surface flow across LI and weak warm advection associated with a temperature difference of 2° – 3°C from southern LI to western CT (Fig. 5a). The surface winds were 15 m s^{-1} over the offshore Atlantic buoys, 10 – 12 m s^{-1} at the southern LI coast, and 7 – 10 m s^{-1} over interior LI. This rapid flow deceleration along the south shore of LI favored frictional convergence of the near-surface flow. A similar wind distribution was located to the north across LIS and southern CT, with 13 – 15 m s^{-1} winds over LIS decelerating to 5 – 10 m s^{-1} just inland of the CT coast. The 4-km MM5 realistically simulated these flow decelerations along both coasts, while the simulated surface temperature gradient was slightly weaker than observed around LI at this time (Fig. 5b).

The low-level winds and boundary layer stratification increased between 1100 and 1400 UTC 1 December 2004, which is illustrated using rawinsonde data at Upton, NY (see OKX in Fig. 1) and ACARS profiles at JFK Airport. The OKX sounding at 1200 UTC 1 December (launched at 1115 UTC) was nearly saturated and moist neutral below 875 mb (Fig. 6a). The south-southeasterly surface winds at 5 m s^{-1} rapidly increased

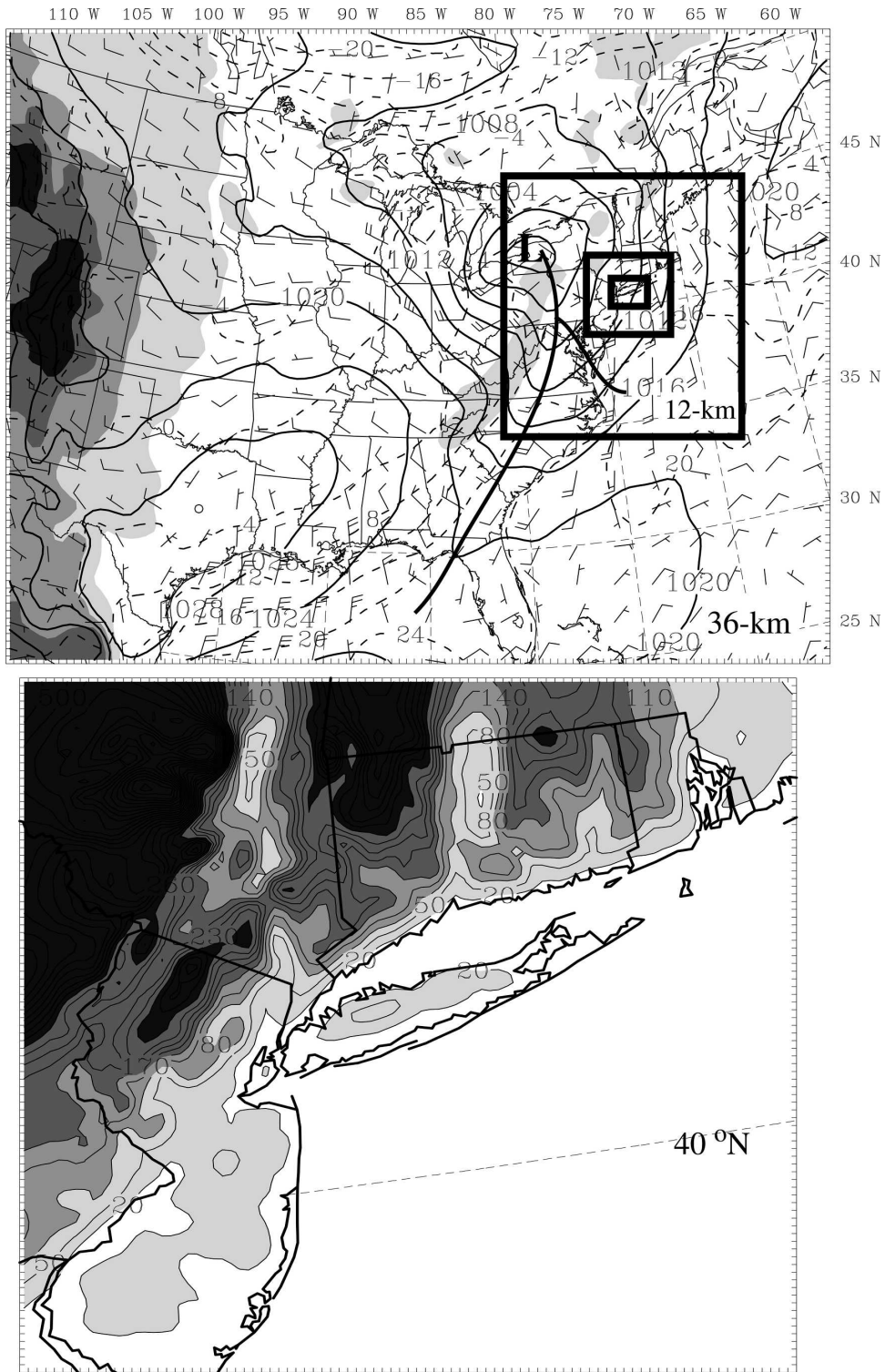


FIG. 3. (a) The 36-km MM5 sea level pressure (solid every 4 mb), 30-m temperature (dashed every 4°C), and winds (full barb = 5 m s⁻¹) at hour 12 (1200 UTC 1 Dec 2004). The MM5 nested domains (12, 4, and 1.33 km) are shown by the three inset boxes. (b) Terrain contoured every 30 m starting at 20 m for the 4-km MM5 domain. Those terrain heights greater than 20, 80, 140, and 280 m are shaded light, medium, dark, and very dark.

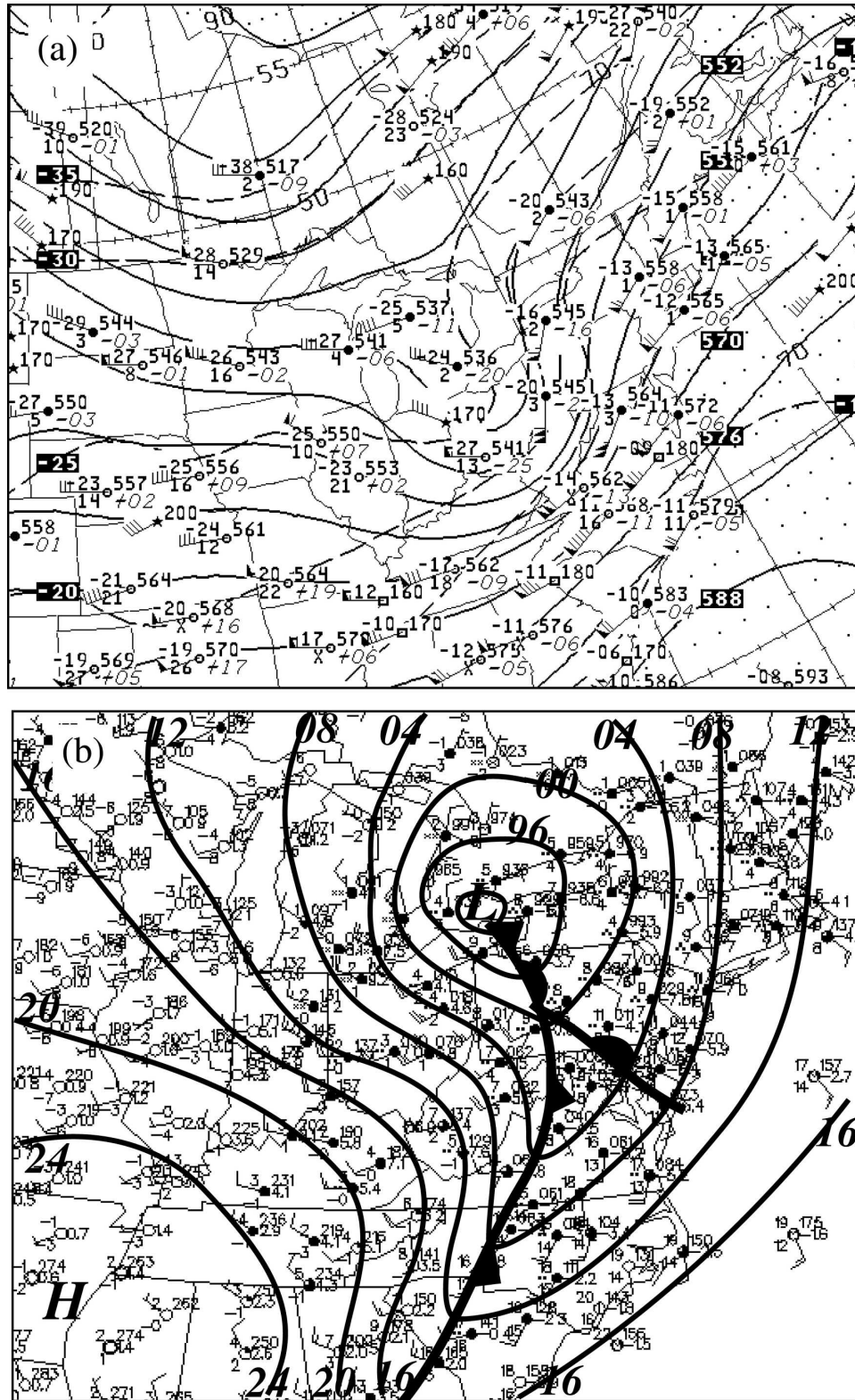


FIG. 4. (a) NCEP 500-mb analysis at 1200 UTC 1 Dec 2004 showing geopotential height (solid every 60 m), temperature (dashed every 5°C), and winds (full barb = 5 m s⁻¹). (b) Manual surface analysis at 1200 UTC 1 Dec 2004 showing sea level pressure (solid every 4 mb) and the station model data (full barb = 5 m s⁻¹).

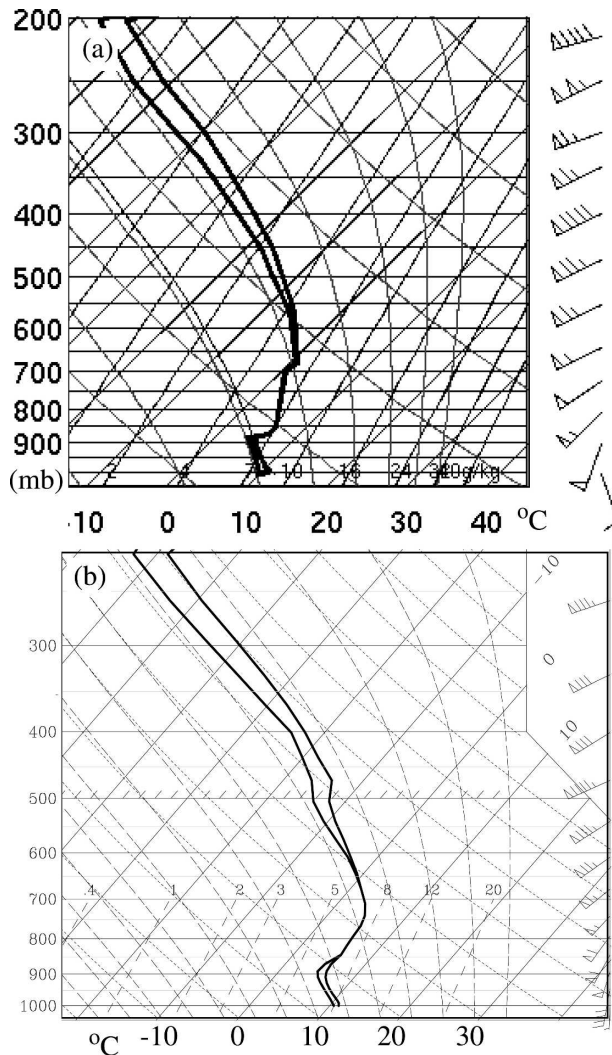


FIG. 6. (a) Sounding at Upton, NY (see OKX in Fig. 1a) at 1200 UTC 1 Dec 2004 showing temperature, dewpoint, and winds (1 full barb = 5 m s^{-1}) on a skew T-log p chart. (b) Same as in (a) except for the 4-km MM5 simulation at hour 12.

with height to 25 m s^{-1} at 900 mb and veered to south-southwesterly at 850 mb. Above this level, southwesterly winds increased to 45 m s^{-1} by 400 mb. The 4-km MM5 also had moist neutral conditions at low levels and a rapid increase in winds to 25 m s^{-1} by 900 mb (Fig. 6b); however, the strength of the stable layer between 900 and 750 mb is somewhat greater than observed.

Meanwhile, around JFK at 1130 UTC 1 December (Figs. 7a,b), both the observed ACARS and 4-km MM5 soundings have lapse rates slightly greater than a moist adiabat within the boundary layer, especially in the model below 950 mb. The height of the stable layer bottom around 900 mb and the low-level wind profile at JFK are similar to the 1200 UTC OKX sounding at this

time. By 1400 UTC (Figs. 7c,d), the low-level stratification at JFK had increased to nearly isothermal on average in the lowest 100 mb. A low-level wind maximum of 35 m s^{-1} was located near the top of this stable layer around 900 mb. The 4-km MM5 winds and low-level stratification were less than observed at this time, but both the observations and model suggest that the stratification and low-level winds were increasing as the precipitation event unfolded.

Figure 8 shows three representative snapshots of the observed low-level precipitation structures around LI between 1000 and 1400 UTC 1 December at 1.0 km MSL for the WSR-88D radar at OKX. At 1000 UTC (Fig. 8a), there was a broad area of light precipitation across much of the region, with embedded areas of moderate precipitation ($>35 \text{ dBZ}$). These areas of heavy precipitation were not collocated with any terrain features at this time. In fact, some of the heaviest precipitation was located over LIS. By 1200 UTC (Fig. 8b), light-to-moderate rainfall (25–30 dBZ) had become more widespread. There was a tendency for the heaviest precipitation ($>30 \text{ dBZ}$) near the coast to extend across western LI as well as along the southwest CT coast. By 1420 UTC (Fig. 8c), the precipitation intensity increased with the approach of the surface occluded front, with a broad area of reflectivities exceeding 35 dBZ to the east of New York City (NYC) and a sharp decrease in precipitation to the west of NYC. The axis of heaviest precipitation tended to conform to the coastal land areas, with the largest reflectivities ($>35 \text{ dBZ}$) over the southwest CT and portions of northern LI. The precipitation ended during the next hour as the surface occluded front crossed the region.

In order to better understand the precipitation evolution and compare it with the model, the 6-h precipitation period (0900–1500 UTC) was separated into three 2-h periods (0900–1100, 1100–1300, and 1300–1500 UTC). An average reflectivity and radial velocity were calculated for several height levels for each 2-h period using the 6-min OKX level-2 data as described in section 2. The 4-km MM5 data at 15-min intervals was also averaged for the same 2-h periods.² For the 0900–1100 UTC period (Fig. 9a), the observed average reflectivity at 0.5 km above mean sea level (MSL) is similar to the 1000 UTC radar snapshot (Fig. 8a), with areas of light to moderate precipitation ($>26 \text{ dBZ}$) to the west of the radar, but no well-defined precipitation enhancement over LI and CT. The model-derived re-

² The model-based reflectivities were calculated using empirical relations based on the model cloud and precipitation mixing ratios (Fovell and Ogura 1988), with modifications to the variable slope intercept for snow based on Thompson et al. (2004).

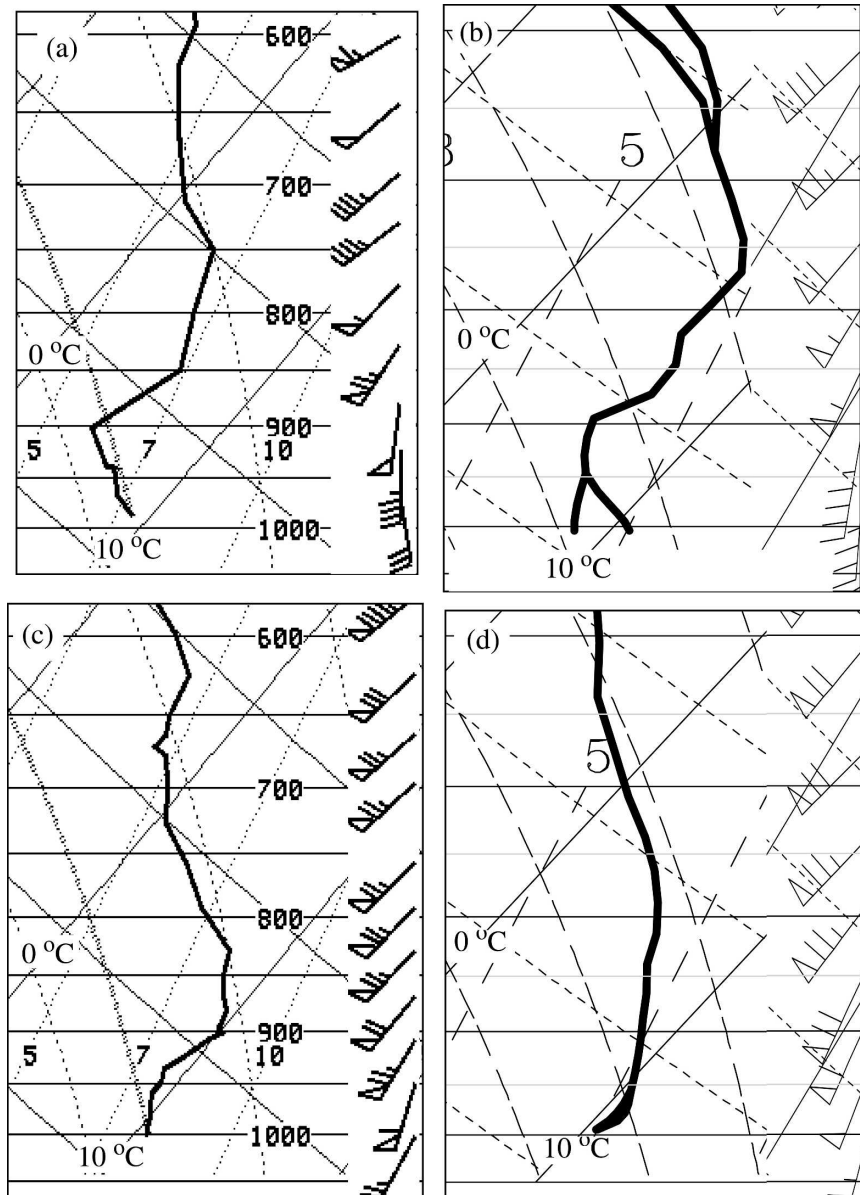


FIG. 7. (a) ACARS temperature and wind profile (full barb = 5 m s^{-1}) on a skew T -log p chart from JFK Airport at 1135 UTC 1 Dec 2004. (b) Same as in (a) except the 4-km MM5 and the dewpoint profile is also shown. (c) Same as in (a) but at 1410 UTC 1 Dec 2004. (d) Same as in (b) but at 1400 UTC 1 Dec 2004.

flectivities at 0.5 km MSL also show little enhancement over the coastal land areas at this time (Fig. 9b), even though there was strong ($\sim 15 \text{ m s}^{-1}$) southerly flow at low levels (Fig. 7).

The average radar cross section (AB) between 0900 and 1100 UTC 1 December from south of LI to southern CT shows enhanced reflectivities in the observations near the bright band (freezing level) around 3 km MSL (Fig. 10a), especially over LIS. As in the observations, there was little precipitation enhancement over

the hills of LI and CT in the model simulation during this period (Fig. 10b). There was little vertical change in potential temperature in the lowest 1 km in the model, which is indicative of the low-level mixed layer in the soundings around this time (cf. Fig. 7), with a stable layer above. As a result of the weak stratification, simulated wind and temperature perturbations were small over LI and shallow sloping ascent was present over coastal hills of CT. An average radial velocity cross section (CD) taken northward from the OKX radar for

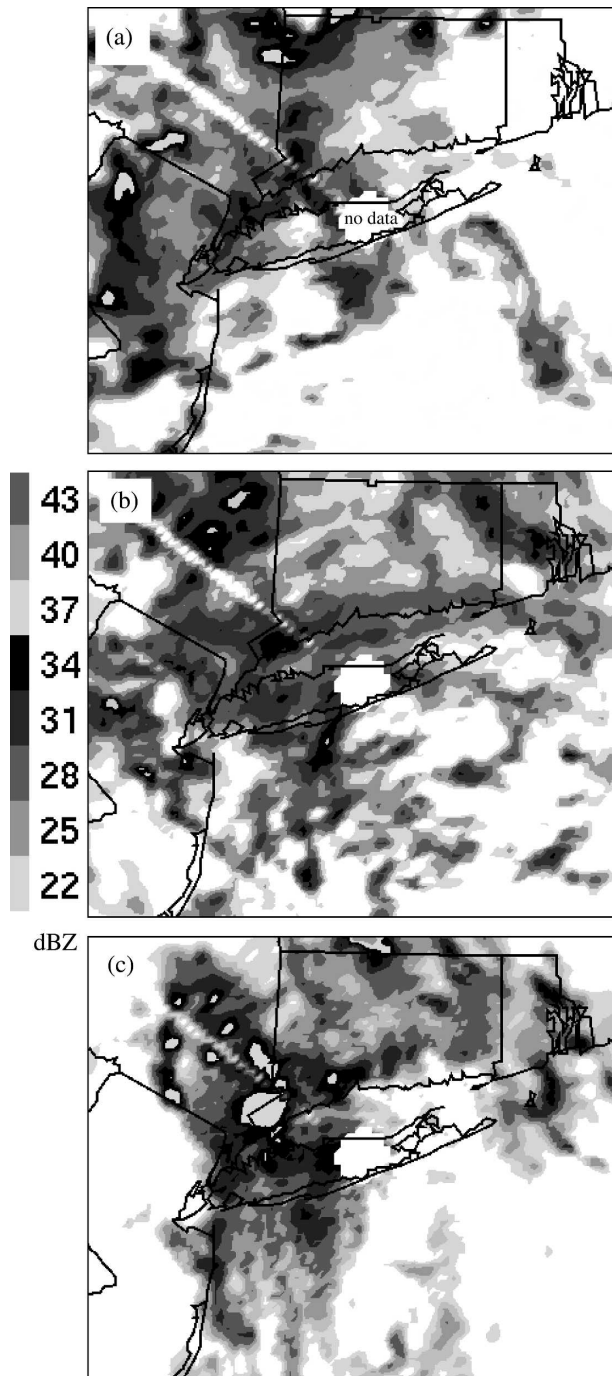


FIG. 8. Low-level (1-km altitude) interpolated radar reflectivity (4-km horizontal grid, shaded every 5 dBZ) from the Upton, NY, WSR-88D radar (OKX in Fig. 1) at (a) 1000, (b) 1200, and (c) 1420 UTC 1 Dec 2004.

this same 2-h period shows a shallow 2 m s^{-1} acceleration over LIS and a 2 m s^{-1} deceleration over coastal CT (Fig. 11a). Overall, during the beginning of this rain event there was little terrain influence on the flow and precipitation perturbations.

For the average 1100–1300 UTC 1 December period (Fig. 9c), the precipitation coverage and intensity had increased at 0.5 km MSL. The reflectivity enhancement ($>30 \text{ dBZ}$) was elongated west–east across central LI and coastal CT. The maximum reflectivity over southeast CT was generally where the coastal terrain was the steepest (Figs. 1 and 3b). In contrast, there was a localized reflectivity minimum ($<27 \text{ dBZ}$) over southern LIS at this level. The 4-km MM5 had a similar reflectivity pattern across CTL (Fig. 9d), although the model reflectivities were 3–4 dBZ larger than observed over western LI and less than observed over eastern LI.

The reflectivity enhancement across section AB over LI and CT extended to approximately 2 km MSL in the radar observations (Fig. 10c). This enhancement was centered over the southern half of LI as well as near the coast of CT, which was well simulated by the 4-km MM5 (Fig. 10d). In this cross section, the observed and simulated reflectivities were 3–4 dBZ weaker over LIS below 2 km MSL than surrounding areas. Interestingly, the observed bright band was still strongest ($>32 \text{ dBZ}$) directly over the low-level precipitation minimum of LIS. The MM5 reflectivity does not produce a bright band, since microphysics scheme cannot produce large aggregated-rimed snowflakes near the freezing level, and the reflectivity algorithm does not include wet melting of snow particles.

The enhanced low-level reflectivity over LI suggests that the vertical terrain circulations had increased during the 1100–1300 UTC period in response to the greater cross-island flow. There is now a more apparent terrain-induced gravity wave in the potential temperatures and vertical circulations over LI, with an upward and downward motion couplet across LI to about 3 km (Fig. 10d). There is slight upstream (southward) tilt with height with the model potential temperature and wind perturbations over LI and coastal CT, which is suggestive of a vertically propagating gravity wave.

Meanwhile, for cross section CD to the north of LI there was a $2\text{--}3 \text{ m s}^{-1}$ deceleration of the southerly flow near coastal CT and a deepening of the shear layer near the coast (Fig. 11b). As a result of the increased surface drag at the coast, the strong low-level jet of 27 m s^{-1} , which was quasi-horizontal over southern LIS, sloped upward over this shear layer at the CT coast. The 4-km MM5 simulation suggests that this sloping shear response was a result enhanced convergence and ascent at the coast as well as a deepening of the boundary layer (not shown), similar to that found in Braun et al. (1999). This sloping shear layer is similar in structure to that described for partially blocked flow over the Cascades and associated orographic precipitation enhancement (Medina et al. 2005); however, unlike their Cas-

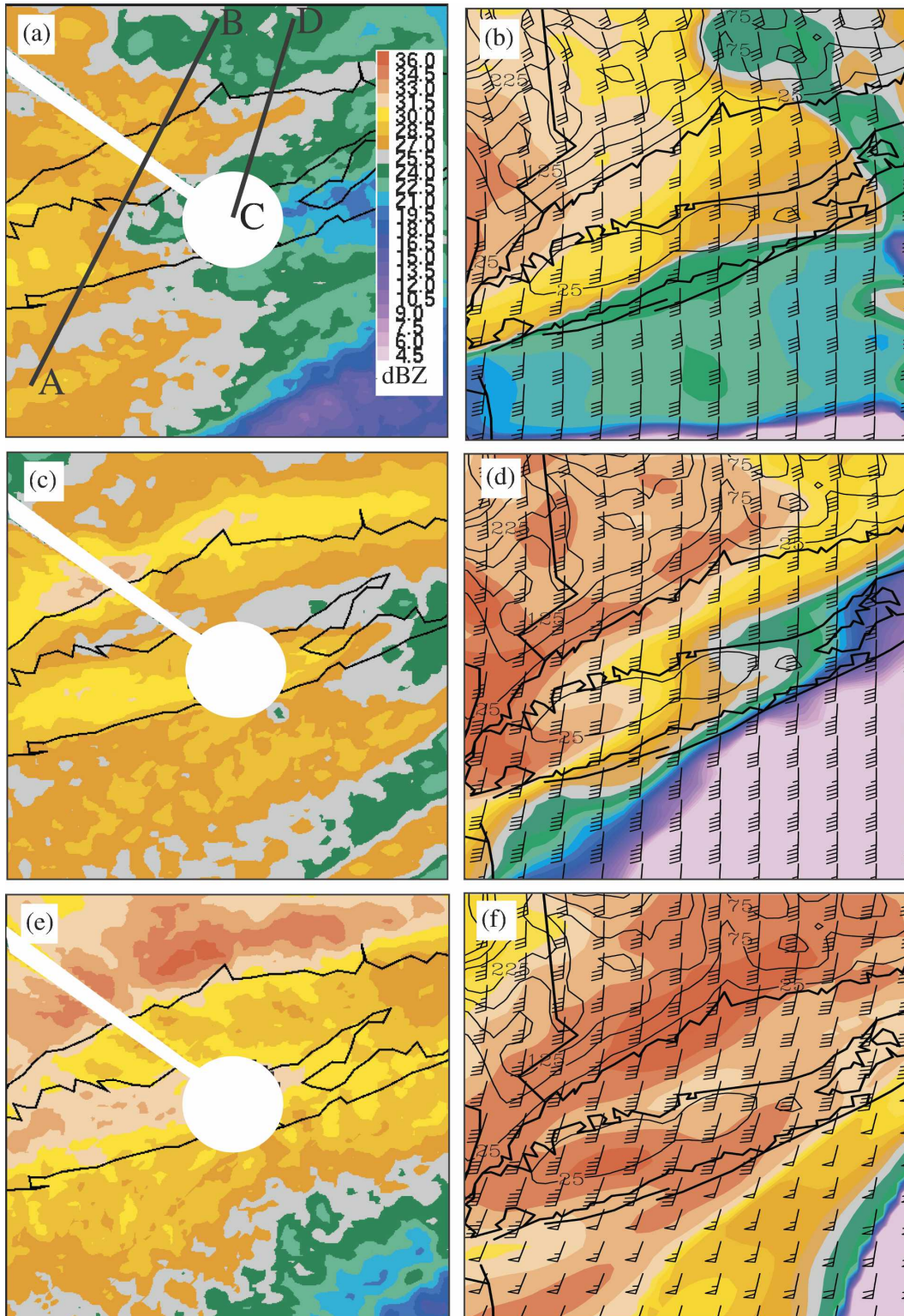


FIG. 9. Two-hour reflectivity average (color shaded every 1.5 dBZ) at 0.5 km MSL from (left) the Upton, NY, WSR-88D radar (OKX on Fig. 1) and (right) derived from the 4-km MM5 from (a), (b) 0900–1100, (c), (d) 1100–1300, and (e), (f) 1300–1500 UTC 1 Dec 2004. The location of cross sections A–B and C–D are shown in (a). MM5 winds (1 full barb = 5 m s^{-1}) at 500 m MSL and terrain (solid lines every 50 m, starting at 25 m) are also shown.

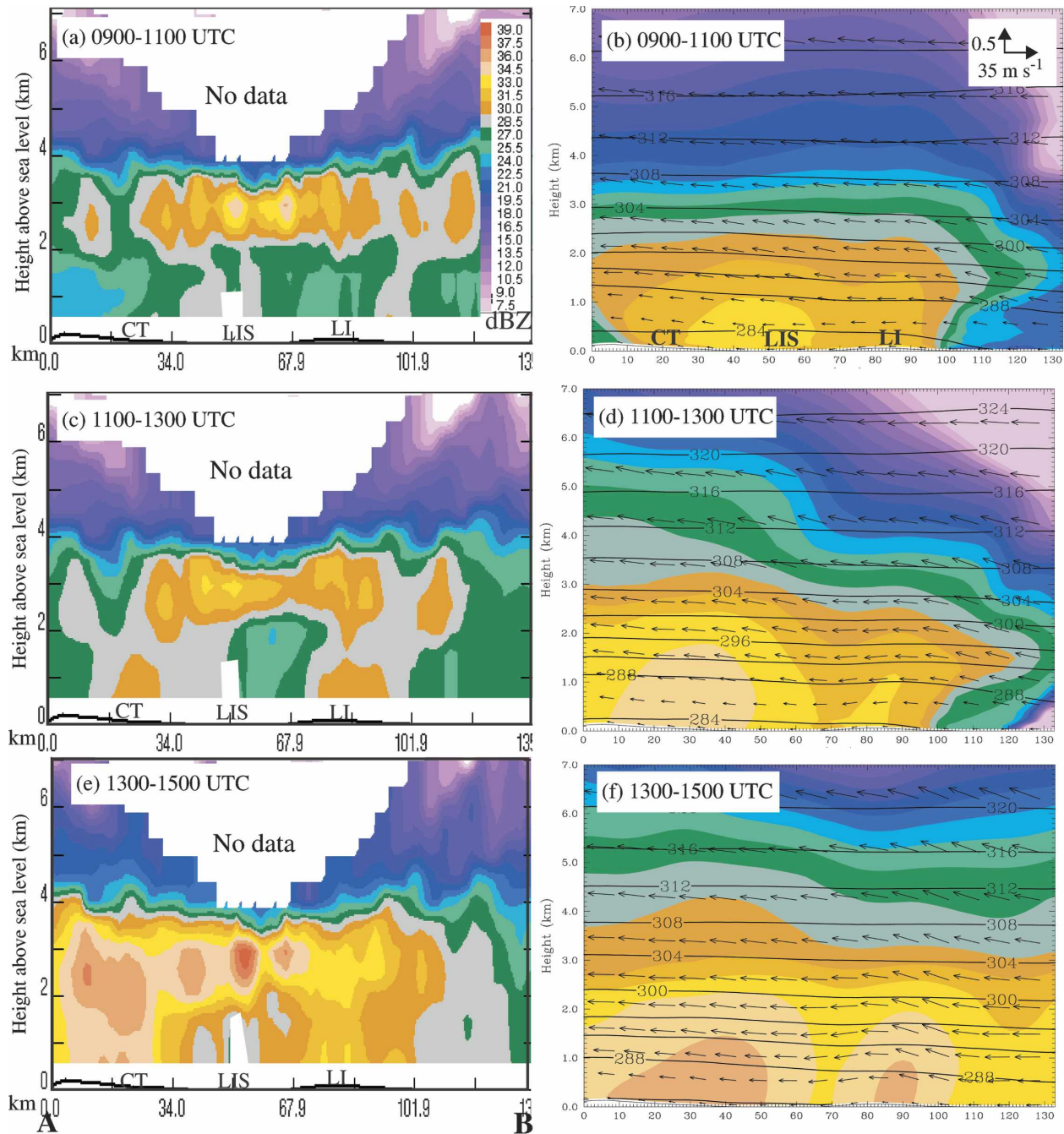


FIG. 10. Cross section A–B showing the 2-h average of the reflectivities (color shaded in dBZ) (left) observed from the Upton, NY, WSR-88D radar (OKX in Fig. 1) and (right) derived from the 4-km MM5 for (a), (b) 0900–1100, (c), (d) 1100–1300, and (e), (f) 1300–1500 UTC 1 Dec 2004. (a)–(f) Shaded every 1.5 dBZ using the scale in (a). The locations of LI, LIS, and CT are labeled. The MM5 circulation in the cross section (vectors) and potential temperature (solid every 4 K) are also shown. The location of the cross section is shown in Fig. 9a.

cases and Alps events, there was no flow blocking over the CT in this case given the relatively small hills and strong flow (Froude number $\gg 1$).

Between 1300 and 1500 UTC 1 December 2001, the precipitation at 0.5 km MSL had intensified by 2–4 dBZ

on average (Fig. 9e), especially over coastal CT. The heaviest precipitation over LI was located over the northern two-thirds of LI, while a minimum in reflectivity persisted over LIS. The 4-km MM5 had a similar precipitation pattern (Fig. 9f); however, the model pre-

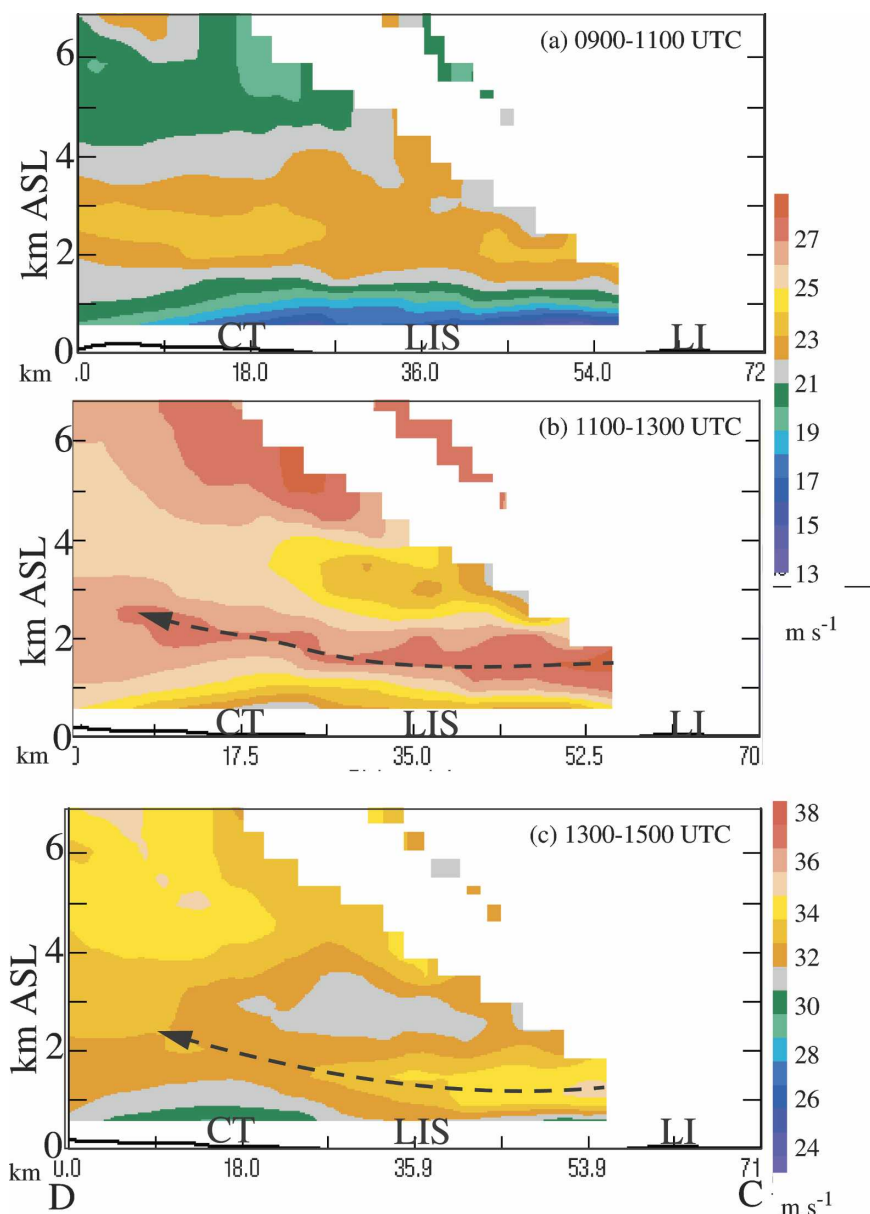


FIG. 11. Cross section C–D showing the 2-h average of the outbound (positive) radial velocities (shaded in m s^{-1}) from the Upton, NY, WSR-88D radar (OKX in Fig. 1) at (a) 0900–1100, (b) 1100–1300, and (c) 1300–1500 UTC 1 Dec 2004. The dashed arrow in (b) and (c) represents the sloping maximum radial velocity below 2 km MSL. The location of the cross section is shown in Fig. 9a.

precipitation enhancement was shifted farther upstream of the southern CT coast than in the observations.

For cross section AB during this 1300–1500 UTC period, both the observed radar and 4-km MM5 still had a precipitation maximum below 2.0 km MSL over LI and coastal CT (Figs. 10e,f). The low-level stratification and flow in the model had increased during the last 2 h, which favored a robust vertical gravity wave circulation around LI, with ascent over the island and descent to

the north over southern LIS. During the 1300–1500 UTC period, the observed radial velocities across CD showed acceleration at around 0.5 km MSL downwind (north) of LI by a few meters per second and then a subsequent deceleration and a deepening of the vertical shear layer over coastal CT (Fig. 11c). The flow's acceleration over southern LIS is associated with low-level divergence and subsidence over southern LIS, while the upward sloping radial velocity field over

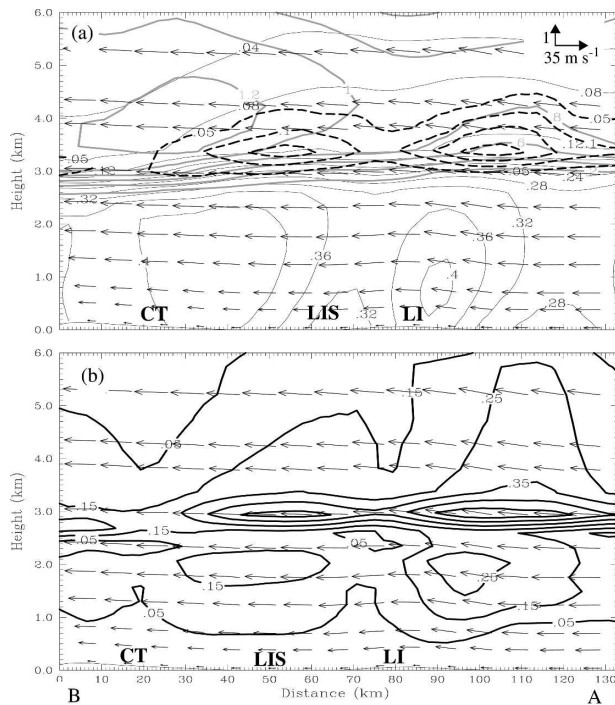


FIG. 12. (a) Model (4 km) cross section A–B showing the 2-h average (1300–1500 UTC) of snow (gray every 0.2 g kg^{-1}), graupel (dashed black every 0.5 g kg^{-1}), rainwater (thin black every 0.04 g kg^{-1}) mixing ratios, as well as the three-dimensional wind circulation vectors in the cross section (see inset scale). (b) Same as in (a) except for cloud water (black every 0.5 g kg^{-1}). The location of the cross section A–B is shown in Fig. 9a.

coastal CT is resulting in the enhanced precipitation over this region. Meanwhile, the subsidence over LIS resulted in a minimum in the observed and simulated radar reflectivities below 2 km MSL over LIS.

To illustrate the 4-km MM5 hydrometeor distribution aloft between 1300 and 1500 UTC, Fig. 12 shows the simulated snow, graupel (rimed snow), rain, and cloud water–mixing ratios across section AB. Below 3 km MSL, there was rain ($>0.35 \text{ g kg}^{-1}$) and cloud water ($>0.15 \text{ g kg}^{-1}$) maxima associated with the upward motions above the southern LI and the coastal CT. The enhanced vertical motions aloft also produced a localized maximum in graupel and cloud water around 3.5 km MSL over the southern LI coast and northern LIS. Meanwhile, between 3 and 4 km MSL the greatest snow ($>1.0 \text{ g kg}^{-1}$) extended northward from LIS to CT. To separate the terrain forcing from the large-scale lift for model hydrometeor production, separate simulations are compared in section 4a without the friction and hills effects.

Figure 13 shows the storm total precipitation for 0600 UTC 1 December (hour 6) to 1800 UTC 1 December (hour 18) from the 4- and 1.33-km grid spacing around

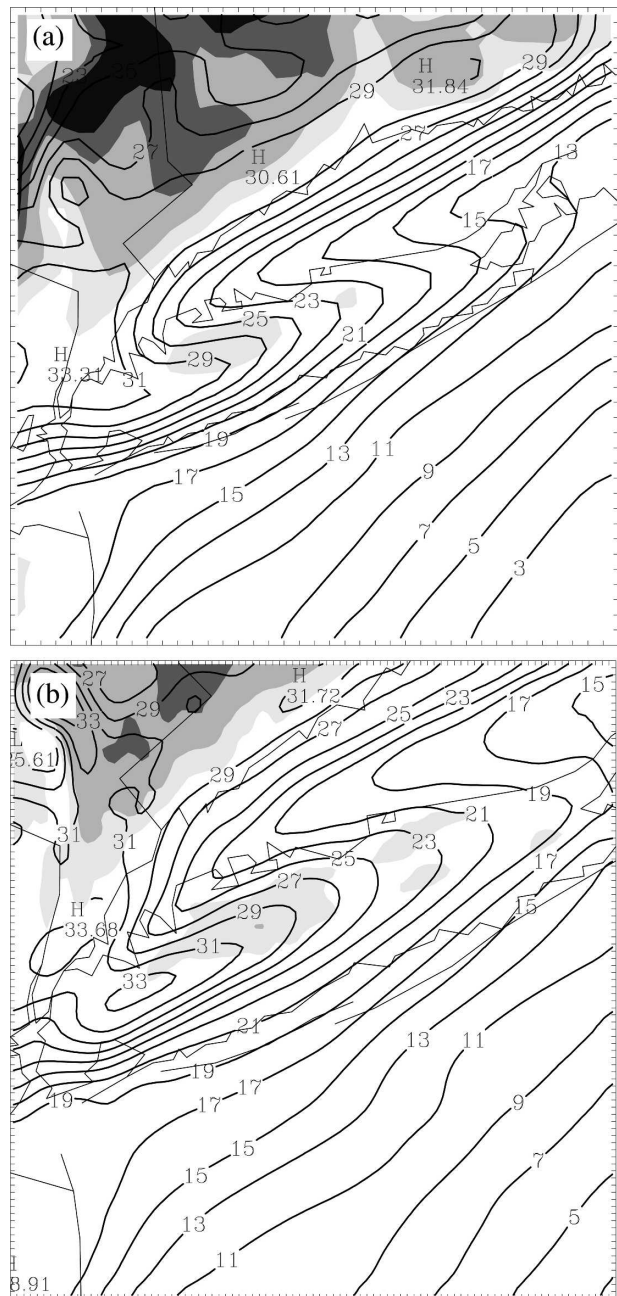


FIG. 13. Model precipitation (solid, mm) between 0600 and 1600 UTC 1 Dec 2004 for the (a) 4- and (b) 1.33-km grid spacings. Model terrain is shaded light, medium, and dark gray at 40, 80, and 150 m MSL, respectively.

LI. The results can be compared with the observed total estimated by radar and the rain gauges (Fig. 2). Both the 4- and 1.33-km MM5 have a similar precipitation enhancement as compared to the observations, with the latter only exceeding 13 mm over the coastal land areas of LI and CT. The precipitation enhancement follows the CT coastline, suggesting that there was both differ-

ential friction and hill effects during the event. Both MM5 resolutions tended to overpredict precipitation to the west around NYC. Since the precipitation structures are similar between the 4- and 1.33-km MM5 runs, the 4-km grid was used for the sensitivity studies in the following section.

4. Discussion

a. Impact of hills and differential friction at the coast

The above results suggest that both the hills and frictional gradients between land and water of near LI and coastal CT were important for the precipitation enhancement. This section focuses on these impacts by conducting additional simulations with these forcings systematically removed. Only the impact of LI was quantified in this section, since the simple island geometry and low hills make it easier to remove model terrain and land features than coastal CT.

The friction and hill effects were isolated by performing a factor separation (Stein and Alpert (1993)). They showed that when more than one factor is considered, it is not sufficient to simply compare a simulation done by removing each physical effect to the control (CTL) simulation, since there can be a net interaction of the two (or more) effects. Therefore, a factor separation for n factors requires 2^n simulations, including the CTL run. For this study, with two factors under consideration (hills and differential friction), this requires three additional simulations besides the CTL run. The first simulation removed LI and replaced it with water (NOLI). The second run allowed the hills to exist, but set the surface drag equal to that over water (LIH2ODRAG). Another simulation replaced the hills over LI with flat land (NOLIHILL). The effect of LI (hills and differential friction together) is given CTL – NOLI. The impact of differential friction at the coast is depicted NOLIHILL – NOLI, while the effect of the hills is given by LIH2ODRAG – NOLI. The interaction between hills and the differential friction is given by [CTL – (NOH2ODRAG + NOLIHILL)] + NOLI. Figure 14a shows the circulation difference between the CTL and NOLI (CTL – NOLI) for cross section A–B averaged between 1300 and 1500 UTC 1 December. The impact of LI results in a 3–5 m s⁻¹ deceleration of the lowest 300 m flow over southern LI. At the southern edge of this deceleration there is low-level convergence and upward motion from the surface up through 6 km, with a maximum of 30 cm s⁻¹ around 1.5 km MSL. Meanwhile, over northern LI the subsidence is of nearly equal amplitude and vertical extent. Long Island also decelerates the near-surface flow downstream (to the north) over LIS and coastal CT. The NOLI run

results in more low-level convergence and upward motion (to 6 cm s⁻¹) at the CT coast, and this upward motion >3 cm s⁻¹ is tilted slightly upwind (south) with height. The increased upward motion over southern LI for the CTL run increases the storm total precipitation over central LI in the 4-km MM5 by 4–5 mm as compared to the NOLI run (Fig. 15a), while decreasing the precipitation over LIS by a nearly equivalent amount.

Figure 14 also shows the circulation differences for the experiments separating the LI hill and differential frictional effects as well as their interaction. The friction over LI decelerates the flow by 1–4 m s⁻¹ below 1 km MSL (Fig. 14c), with some of this deceleration extending northward below 0.5 km toward CT. Both hills and differential friction are important to the vertical circulation over LI, with nearly half the total vertical motion enhancement below 3.5 km coming from the hills (Fig. 14b), and the other half from the frictional convergence and divergence along the southern and northern LI coasts, respectively (Fig. 14c). Above 3.5 km MSL and to the north of LI the vertical motion associated with the hills is about 30%–40% larger than frictional forcing. The frictional forcing contributes to a broader area of subsidence over LIS than the hill forcing. The interaction between friction and hill effects results in only a 5%–10% contribution to the net vertical motion produced by LI (Fig. 14d). It is generally of opposite sign to the hills and friction effects, since friction acts to slow the boundary layer flow and therefore results in a weaker hill-induced circulation.

As compared to the total impact of LI on the precipitation (Fig. 15a), the impact of differential friction explains about 53% of the total LI precipitation difference (Fig. 15b), while the hills explain about 43% (Fig. 15c). The interaction of the two processes results in little impact (<5%) of the precipitation (not shown).

The simulated upward motion over the southern LI coast for the differential friction impacts (cf. Fig. 14c) can be compared with that estimated using scale analysis. Passarelli and Boehme (1983) estimated the vertical motion (w) from frictional convergence using the scaling:

$$w \approx \frac{H}{L} \Delta u, \quad (1)$$

where H is the depth of the atmosphere over which the wind speed is reduced by Δu and L is the horizontal length scale. Therefore, The model deceleration (Δu) of 3 m s⁻¹ within the lowest 300 m (H) over a 10-km distance (L) results in an approximate w of 9 cm s⁻¹, which is close to the simulated frictional response below 1 km (Fig. 14c).

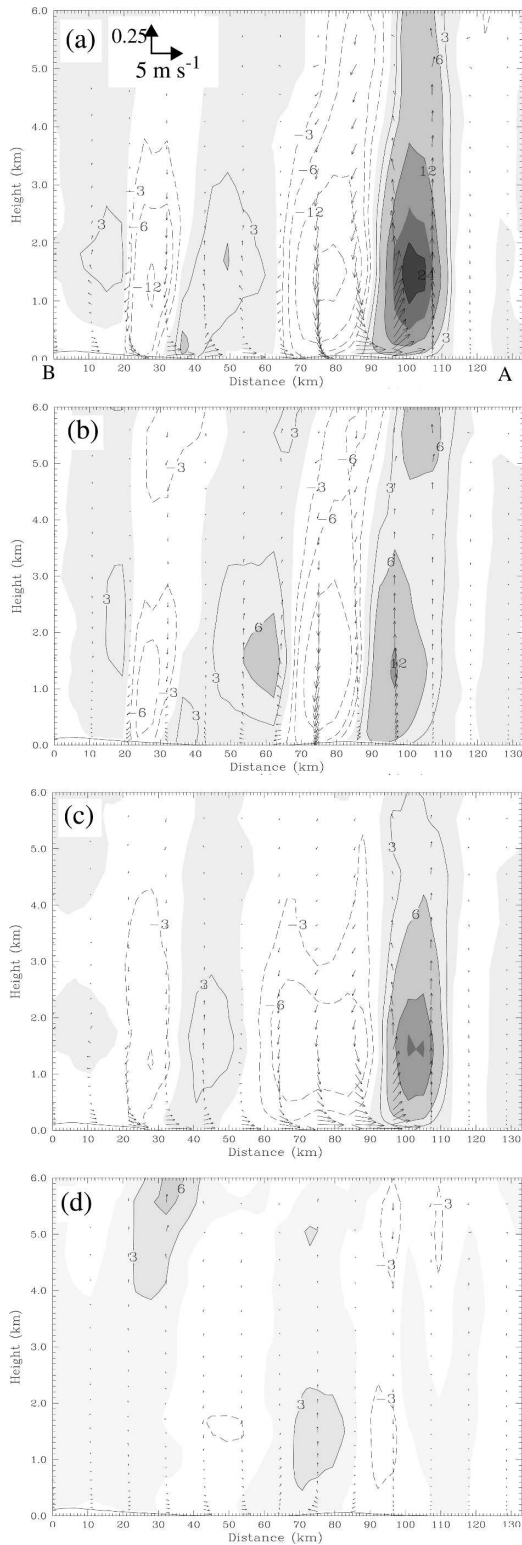


FIG. 14. Difference plot for section A–B showing (a) CTL – NOLI (impact of LI), (b) LIH2ODRAG – NOLI (impact of hills), (c) NOLIHILL – NOLI (impact of frictional convergence), and (d) interaction between hills and friction showing circulation and vertical motion (shaded = upward; dashed downward every 3 cm s^{-1}).

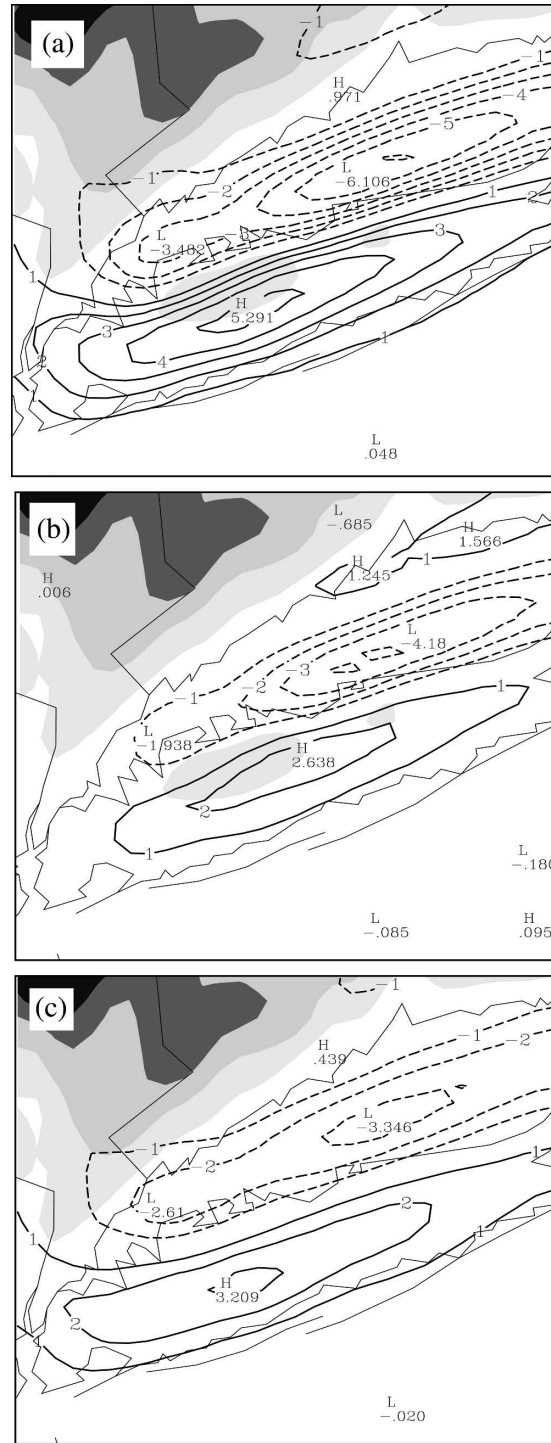


FIG. 15. Difference plot of storm total (0600–1800 UTC 1 Dec 2004) precipitation (every 1 mm) for the (a) CTL – NOLI (impact of LI), (b) LIH2ODRAG – NOLI (impact of LI hills), and (c) NOLIHILL – NOLI (impact of frictional convergence). Negative differences are dashed. Terrain from the 4-km MM5 is shaded at 40, 100, 150, and 200 m.

The vertical extent of the circulation over LI for the hills and differential friction effects is consistent with that of a gravity wave. These waves were generated by either stably stratified flow perturbed by the hills or by the upward motion induced by the frictional convergence at the coast (Fig. 14c). The hill circulations are somewhat more robust with height than the differential friction, thus suggesting that the hills were a slightly more dominant wave forcing. The axes of maximum and minimum ascent/descent associated with the hill forcing tilt slightly upstream with height, which is consistent with a linear gravity wave (Durran 1986). For a wave to propagate vertically, the frequency generated by the flow over the terrain must be less than or equal to the static stability, that is Uk or $2\pi U/a$ is $\leq N$, with a defined as the mountain half-width and N the moist static stability (Durran and Klemp 1982). The average moist N below 1000 m was $\sim 0.015 \text{ s}^{-1}$ at 1400 UTC given the stable layer below 900 mb (Figs. 8c,d), while $Uk \sim 0.0125 \text{ s}^{-1}$, with $U \sim 25 \text{ m s}^{-1}$ and $a = 15 \text{ 000 m}$. Typically, the narrow terrain of LI would favor evanescent waves under most strong flow conditions; however, the increased stratification later in this December event allowed for vertically propagating waves and deeper vertical motion response.

These results suggest that even the differential friction at the coast and relatively narrow and low hills can generate gravity waves under stable and strong flow conditions. A similar differential frictional response for a coastal boundary was also found using two-dimensional idealized model (Braun et al. 1999). Using aircraft observations Garvert et al. (2005, 2006, manuscript submitted to *Mon. Wea. Rev.*) showed that the 300–500-m terrain ridges over the windward foothills of the Oregon Cascades led to significant vertical motions and cloud water generation associated with terrain-induced gravity waves.

The sloping shear layer and ascent over southern CT in the radar radial velocities is similar to recent studies from regions with more significant topography, such as the windward Cascade mountains and Alps (Medina et al. 2005). For these steeper mountain barriers, this sloping momentum field and precipitation enhancement was attributed to the windward high pressure perturbation associated with upstream flow blocking. The CT hills are too small to generate a significant windward pressure perturbation. However, these results suggest that one can generate a similar upward sloping or deepening shear layer when there is a large horizontal increase in the surface roughness and deepening of the boundary layer, which occurred for this case as near-surface flow crossed from LIS to CT (Figs. 11b,c). A

similar response was found in the idealized simulations of flow past a coastal boundary in Braun et al. (1999).

b. Low-level precipitation enhancement

The “classic” seeder-feeder mechanism described by Browning et al. (1975) is one in which the low-level feeder cloud has sufficient moisture and vertical motion to form cloud-sized particles but not precipitation-sized particles. Hence, precipitation would not occur without the presence of the precipitation-sized seeder ice particles falling from the seeder cloud into the feeder cloud and growing by accretion of cloud particles within the feeder cloud.

The radar observations across LI and CT for this 1 December event indicate precipitation-sized ice particle aloft and enhanced reflectivities in the lowest 2–3 km over LI and CT (cf. Fig. 10). The goal of this section is to illustrate how well this case represents the “classical” seeder-feeder model. To better quantify the growth of precipitation within the three-dimensional storm volume, Fig. 16 presents accumulated contoured frequency by altitude diagrams (CFADs; Yuter and Houze 1995) of observed radar reflectivity from each volume above the LI and LIS regions for the period from 1100 to 1300 UTC 1 December. The CFADs show increasing reflectivity with decreasing height above 4-km altitude, thus indicating precipitation growth in the ice layer over both LI and LIS. The distribution is narrower (tighter contours) and shifted to slightly lower reflectivity values for LIS as compared to LI indicating a more uniform distribution of reflectivities at a given height and slightly lower modal reflectivities for ice over LIS. The reflectivities associated with mixed precipitation in the brightband peak at 3.5-km altitude. Below 2-km altitude, the rain layer has slightly higher modal reflectivities over LI (~ 2 dB larger, corresponding to $\sim 25\%$ increase in the rain rate) compared to LIS. There is also a slight diagonal slant to the mode in the rain layer over LI, indicating some growth of precipitation in the rain layer. In contrast, there is a more vertical mode to the reflectivity in the rain layer for LIS, indicating little to no growth.

The microphysical impacts of LI in the model were quantified by calculating the difference in rain, snow, graupel (rimed snow), and cloud water–mixing ratios aloft between the CTL and NOLI runs (Fig. 17). The CTL produces 0.03 – 0.09 g kg^{-1} more rain via cloud water accretion over southern LI from the surface to the freezing level (~ 3 km; Fig. 17b), while there is a reduction of rain via subsidence over LIS by a similar amount. This rain difference represents about 10%–30% of the total in the CTL (Fig. 12a). Given the large vertical extent of the upward motion differences be-

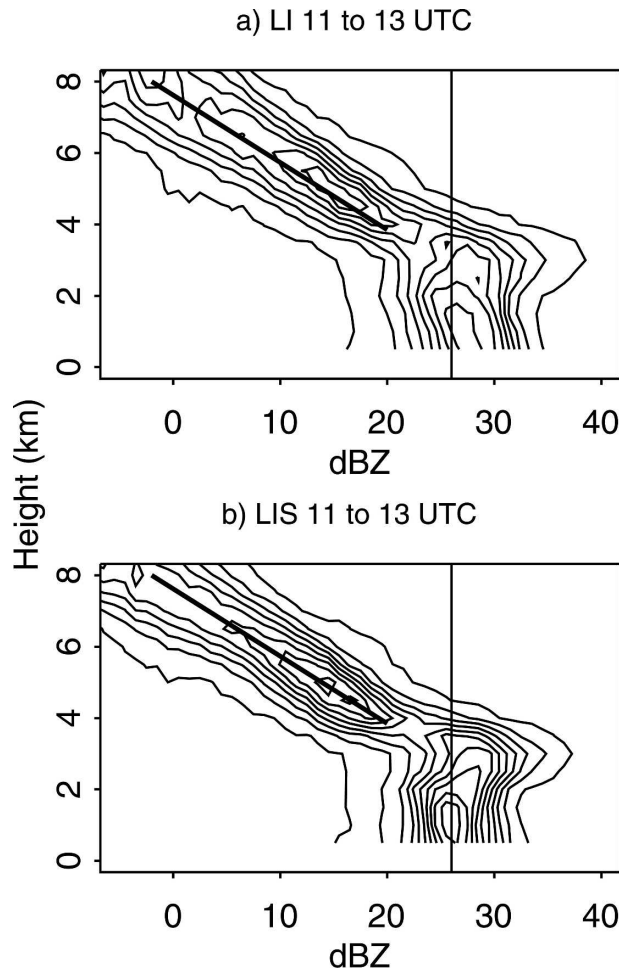


FIG. 16. Accumulated CFADs of observed reflectivity over (a) LI and (b) LIS from 1100 to 1300 UTC 1 Dec 2001. The vertical line is at 26 dBZ. Diagonal line is the same in both parts and is centered on modal reflectivity in the ice layer for the LIS CFAD. The CFAD bin size is 1 dBZ.

tween the CTL and NOLI, there is also $0.01\text{--}0.05\text{ g kg}^{-1}$ more rimed snow in the CTL between 3 and 5 km MSL over southern LI, while there is less rimed snow over LIS within this same layer aloft. This 10%–20% reduction in rimed snow in the NOLI is the result of greater or less riming where there is enhanced upward and downward motion, respectively. The amount of riming is dependent on the cloud water, which is increased slightly over southern LI in the CTL, while it is decreased over LIS. The increased riming over southern LI at 4 km MSL also reduces the dry snow by $0.02\text{--}0.04\text{ g kg}^{-1}$. The upward motion differences above 5 km also results in a slight ($0.02\text{--}0.04\text{ g kg}^{-1}$) increase and decrease in dry snow over LI and LIS, respectively; however, this snow difference aloft only represents less than 5% of the total snow aloft (Fig. 12a). Therefore, the

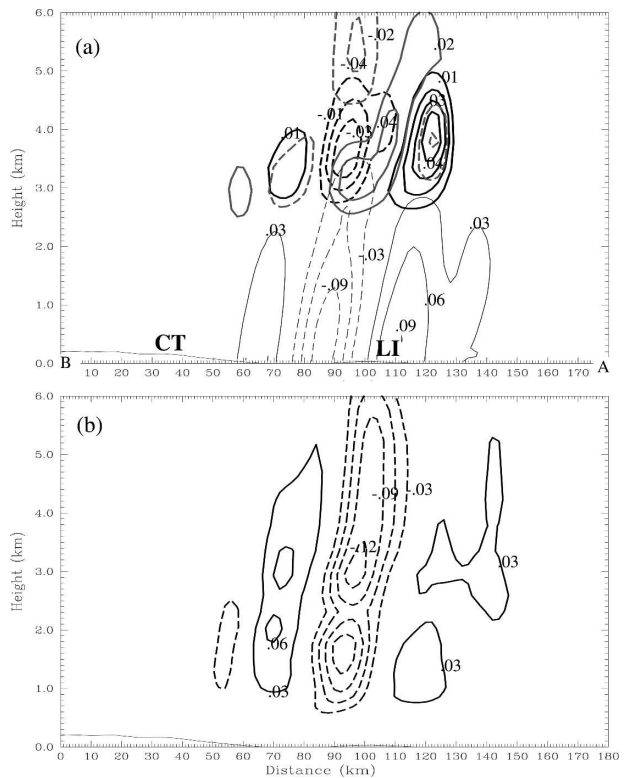


FIG. 17. Difference plot along section A–B for the 1300–1500 UTC 1 Dec 2004 average for CTLNOLI showing mixing ratio differences of (a) rainwater (thin black every 0.03 g kg^{-1}), snow (gray every 0.02 g kg^{-1}), and rimed snow (thick black every 0.01 g kg^{-1}). The negative difference values are dashed. (b) Same as in (a) but for cloud water (black every 0.03 g kg^{-1}). The location of the cross section A–B is shown in Fig. 9a.

hills and differential friction effects of LI did not have significant impact on the seeder cloud, since the large-scale frontal ascent generated most of the ice aloft.

To quantify the seeder-feeder impact on precipitation for the 1 December 2004 case, a separate 4-km MM5 simulation (NOSEEDER) was completed in which the hydrometeors generated above 3 km MSL were not allowed to increase the snow/water mass above this level, but the supersaturation removal and latent heating/cooling effects were still allowed, so that the flow dynamics were not altered much. The boundary conditions for this 4-km run were from the 12-km CTL run, but the ice and water tendencies along the lateral 4-km domain boundaries above 3 km MSL were set to zero. For the 1300–1500 UTC 1 December average (Fig. 18a), the lack of ice aloft, and hence lack of seeder particles falling through the lower-level cloud, increases the cloud water between 2–3 MSL by nearly a factor of 2 (Fig. 13b), since there are fewer particles to collect cloud water by accretion. Associated with the increase in cloud water is a decrease in the average

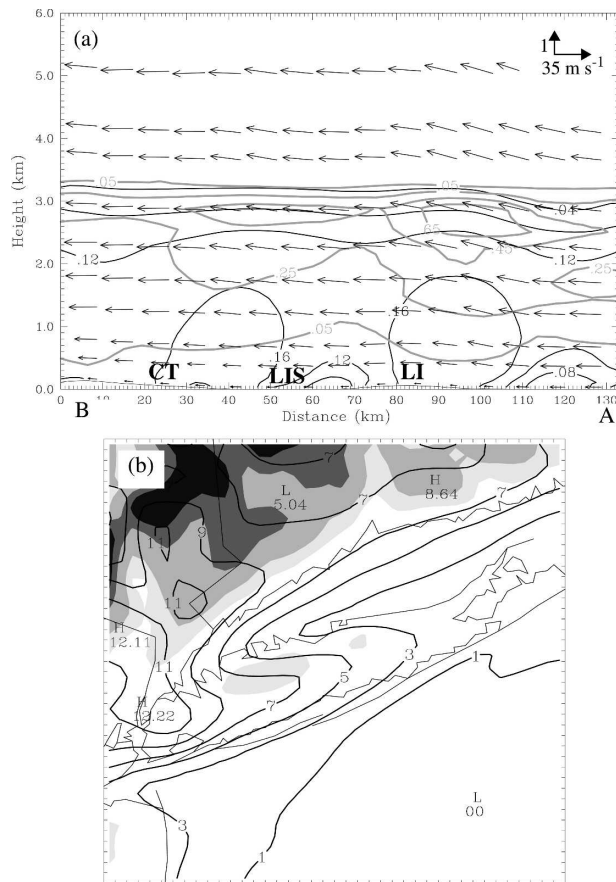


FIG. 18. (a) Same as in Fig. 12a but for the NOSEEDER experiment showing rain (black every 0.04 g kg^{-1}) and cloud water (gray every 0.05 g kg^{-1}) mixing ratios, as well as wind circulation vectors in the cross section. (b) Same as in Fig. 13a but for the NOSEEDER experiment showing precipitation every 2 mm.

rainwater below 3 km MSL by a factor of 2 as compared to the CTL run (cf. Fig. 12a). This sensitivity test shows that the seeder-feeder mechanism was the dominant but not exclusive source of rainwater at low levels. NOSEEDER had a factor of 4 decrease in surface rainfall compared to CTL (Figs. 18b and 13a). The feeder (water) cloud was still able to precipitate given its 3-km depth and sufficient upward motion (estimated in the MM5 simulation at $10\text{--}30 \text{ cm s}^{-1}$ at 4 km^2 horizontal scale). Therefore, this case does not represent a classic seeder-feeder mechanism, but rather a superposition of a seeder-feeder mechanism and processes excluding ice particles within the low-level cloud.

5. Conclusions

The relatively small hills of Long Island (LI; 50–100 m) and coastal Connecticut (CT; 100–300 m) as well as the differential friction across the coast are shown to

produce a 30%–40% enhancement of the precipitation on 1 December 2004. This study uses WSR-88D radar observations at Upton, New York, to better understand the vertical structure of the precipitation over the region as well as the low-level flow just above the surface. The radar and other conventional observations are compared with a nested 4-km simulation using the fifth-generation Pennsylvania State University–National Center for Atmospheric Research (PSU–NCAR) Mesoscale Model (MM5). Sensitivity simulations removing the LI hills and land areas are used to quantify the relative importance of both of these processes.

The precipitation enhancement developed as the strong ($>15 \text{ m s}^{-1}$) surface southerly flow to the east of an approaching extratropical cyclone interacted with coastal southern New England. The low-level stratification also increased during the event as warm advection ahead of a weak warm front occurred above the surface. As the flow and stability increased during the event, precipitation enhancement of 2–3 dBZ developed from the surface upward to around the freezing level (3 km MSL) across central LI and southern CT, while there was a localized precipitation minimum over LI Sound. The MM5 realistically produced these precipitation structures, and was within 10%–20% of the surface precipitation in many areas.

The MM5 produced a terrain-forced gravity wave over the hills of LI and coastal CT to 6 km MSL as the cross-hill flow and stratification increased during the event. The waves are shown to produce a $10\text{--}30 \text{ cm s}^{-1}$ enhancement of the upward motion over southern LI and CT, while there was subsidence of a nearly equal amount of the LI Sound. This resulted in significant modifications to the rain and cloud water below the freezing level ($\sim 3 \text{ km MSL}$) where vertical motion were largest ($10\text{--}30 \text{ cm s}^{-1}$) and the associated accretional growth of precipitation was most active; however, there was little change to the amount of snow cloud aloft, where the vertical motion perturbations were around $4\text{--}8 \text{ cm s}^{-1}$. Overall, this resulted in a deeper precipitation enhancement than previous studies over the small ($<100 \text{ m}$) hill. Unlike the classic seeder-feeder conceptualization, a MM5 sensitivity run suggests that the feeder cloud was able to precipitate without the seeder cloud above 3 km; however, the seeder ice aloft was important in increasing accretional growth in the rain layer, such that surface precipitation was enhanced by a factor of 4.

Sensitivity MM5 simulations were performed for LI to isolate the impact of small hills, differential friction across the coast, and their interaction. Both the hills and frictional effects contribute nearly equally to the total precipitation enhancement and the vertical circu-

lations below 3 km. The hills enhance the gravity wave circulations slightly more than the frictional effects above 3 km, but both the hills and frictional effects had little impact on the snow cloud aloft. The interaction of differential friction and hill effects had little impact on the vertical circulation and precipitation across LI.

The sloping shear layer and its ascent over southern CT in the radar radial velocities are similar to recent orographic precipitation studies from regions with more significant topography, such as the windward Cascade Mountains and Alps. This suggests that this sloping shear layer can develop as a result of differential friction at the coast as well as for low-level flow blocking for high mountains, as shown in previous studies.

Overall, this study has shown the utility of comparing composite averages of high-resolution WSR-88D data in three dimensions with high-resolution model simulations in order to illustrate important terrain-forced precipitation structures in relation to the flow. Rather than using the conventional snapshots of WSR-88D data along constant elevation beam angles, compositing the radar along constant height surfaces can reveal more of the time mean structures that can be compared more easily with model simulations. Future work will utilize this approach to look at orographic precipitation structures between the model and observed over more significant terrain. Meanwhile, a longer-term model and observed climatology of the radar and model precipitation is needed along the coastlines where both differential friction and hills are important.

Acknowledgments. This research was supported by the National Science Foundation (ATM-0450444 for Colle and ATM-0121963 for Yuter) and the COMET-Cooperative Program (Grant S0238662). We wish to thank the two anonymous reviewers for helping to improve the manuscript. Use of the MM5 was made possible by the Microscale and Mesoscale Meteorological (MMM) Division of NCAR, which is supported by the National Science Foundation. The second author gratefully acknowledges J. Kane for simulating her interest in the environmental science of Long Island.

REFERENCES

- Bader, M. J., and W. T. Roach, 1977: Orographic rainfall in warm sectors of depressions. *Quart. J. Roy. Meteor. Soc.*, **103**, 269–280.
- Barnes, S. L., 1980: Report on a meeting to establish a common Doppler radar data exchange format. *Bull. Amer. Meteor. Soc.*, **61**, 1401–1404.
- Barros, A. P., and R. J. Kuligowski, 1998: Orographic effects during a severe wintertime rainstorm in the Appalachian Mountains. *Mon. Wea. Rev.*, **126**, 2648–2672.
- Bergeron, T., 1949: The problem of artificial control of rainfall on the globe. Part II: The coastal orographic maxima of precipitation in autumn and winter. *Tellus*, **1**, 15–32.
- , 1960: Operation and results of “Project Pluvius.” *Physics of Precipitation, Geophys. Monogr.*, Vol. 5, Amer. Geophys. Union, 152–157.
- Braun, S. A., R. Rotunno, and J. B. Klemp, 1999: Effects of coastal orography on landfalling cold fronts. Part II: Effects of surface friction. *J. Atmos. Sci.*, **56**, 3366–3384.
- Browning, K. A., 1980: Structure, mechanism and prediction of orographically enhanced rain in Britain. *Orographic Effects in Planetary Flows*, R. Hide and P. W. West, Eds., GARP Publication Series, Vol. 23, World Meteorological Organization, 85–114.
- , C. W. Pardoe, and F. F. Hill, 1975: The nature of orographic rain at wintertime cold fronts. *Quart. J. Roy. Meteor. Soc.*, **101**, 333–352.
- Colle, B. A., J. B. Olson, and J. S. Tongue, 2003: Multiseason verification of the MM5. Part I: Comparison with the NCEP Eta Model over the central and eastern United States and impact of MM5 resolution. *Wea. Forecasting*, **18**, 431–457.
- Corbet, J., C. Mueller, C. Burghart, K. Gould, and G. Granger, 1994: Zeb: Software for integration, display, and management of diverse environmental datasets. *Bull. Amer. Meteor. Soc.*, **75**, 783–792.
- Dudhia, J., 1989: Numerical study of convection observed during the Winter Monsoon Experiment using a mesoscale two-dimensional model. *J. Atmos. Sci.*, **46**, 3077–3107.
- Durran, D. R., 1986: Mountain waves. *Mesoscale Meteorology and Forecasting*, P. S. Ray, Ed., Amer. Meteor. Soc., 472–492.
- , and J. B. Klemp, 1982: On the effects of moisture on the Brunt–Väisälä frequency. *J. Atmos. Sci.*, **39**, 2152–2158.
- Fovell, R. G., and Y. Ogura, 1988: Numerical simulation of a mid-latitude squall line in two dimensions. *J. Atmos. Sci.*, **45**, 3846–3879.
- Garvert, M. F., B. A. Colle, and C. F. Mass, 2005: The 13–14 December 2001 IMPROVE-2 event. Part I: Synoptic and mesoscale evolution and comparison with a mesoscale model simulation. *J. Atmos. Sci.*, **62**, 3474–3492.
- Grell, G. A., J. Dudhia, and D. R. Stauffer, 1994: A description of the fifth-generation Penn State/NCAR Mesoscale Model (MM5). NCAR Tech. Note NCAR/TN-398+STR, 138 pp. [Available from National Center for Atmospheric Research, P. O. Box 3000, Boulder, CO 80307.]
- Hill, F. F., K. A. Browning, and M. J. Bader, 1981: Radar and raingauge observations of orographic rain over South Wales. *Quart. J. Roy. Meteor. Soc.*, **107**, 643–670.
- Hong, S.-Y., and H.-L. Pan, 1996: Nonlocal boundary layer vertical diffusion in a medium-range forecast model. *Mon. Wea. Rev.*, **124**, 2322–2339.
- Houze, R. A., Jr., 1993: *Cloud Dynamics*. Academic Press, 573 pp.
- James, C. N., S. R. Brodzik, H. Edmon, R. A. Houze Jr., and S. E. Yuter, 2000: Radar data processing and visualization over complex terrain. *Wea. Forecasting*, **15**, 327–338.
- Klemp, J. B., and D. R. Durran, 1983: An upper boundary condition permitting internal gravity wave radiation in numerical mesoscale models. *Mon. Wea. Rev.*, **111**, 430–444.
- Medina, S., B. F. Smull, R. A. Houze Jr., and M. Steiner, 2005: Cross-barrier flow during orographic precipitation events: Results from MAP and IMPROVE. *J. Atmos. Sci.*, **62**, 3580–3598.
- Miller, J. F., and R. H. Frederick, 1969: The precipitation regime of Long Island, New York: Hydrology and some effects of

- urbanization in Long Island, New York. U.S. Geological Survey, Professional Paper 627-A, 21 pp.
- Novak, D., and B. A. Colle, 2006: Observations of multiple sea-breeze boundaries during an unseasonably warm day in metropolitan New York City. *Bull. Amer. Meteor. Soc.*, **87**, 169–174.
- Passarelli, R. E., Jr., and H. Boehme, 1983: The orographic modulation of pre-warm front precipitation in southern New England. *Mon. Wea. Rev.*, **111**, 1062–1070.
- Smith, R. B., 1979: The influence of mountains on the atmosphere. *Advances in Geophysics*, Vol. 21, Academic Press, 87–233.
- Stein, V., and P. Alpert, 1993: Factor separation in numerical simulations. *J. Atmos. Sci.*, **50**, 2107–2115.
- Storebo, P. B., 1976: Small scale topographic influences on precipitation. *Tellus*, **28**, 45–59.
- Thompson, G., R. M. Rasmussen, and K. Manning, 2004: Explicit forecasts of winter precipitation using an improved bulk microphysics scheme. Part I: Description and sensitivity analysis. *Mon. Wea. Rev.*, **132**, 519–542.
- Yuter, S. E., and R. A. Houze Jr., 1995: Three-dimensional kinematic and microphysical evolution of Florida cumulonimbus. Part II: Frequency distributions of vertical velocity, reflectivity, and differential reflectivity. *Mon. Wea. Rev.*, **123**, 1941–1963.